

Proximity effect on spin-dependent conductance and thermopower of correlated quantum dots

Krzysztof P. Wójcik* and Ireneusz Weymann†

Faculty of Physics, Adam Mickiewicz University, ul. Umultowska 85, 61-614 Poznań, Poland

(Dated: January 16, 2022)

We study the electric and thermoelectric transport properties of correlated quantum dots coupled to two ferromagnetic leads and one superconducting electrode. Transport through such hybrid devices depends on the interplay of ferromagnetic-contact induced exchange field, superconducting proximity effect and correlations leading to the Kondo effect. We consider the limit of large superconducting gap. The system can be then modeled by an effective Hamiltonian with a particle-non-conserving term describing the creation and annihilation of Cooper pairs. By means of the full density-matrix numerical renormalization group method, we analyze the behavior of electrical and thermal conductances, as well as the Seebeck coefficient as a function of temperature, dot level position and the strength of the coupling to the superconductor. We show that the exchange field may be considerably affected by the superconducting proximity effect and is generally a function of Andreev bound state energies. Increasing the coupling to the superconductor may raise the Kondo temperature and partially restore the exchange-field-split Kondo resonance. The competition between ferromagnetic and superconducting proximity effects is reflected in the corresponding temperature and dot level dependence of both the linear conductance and the (spin) thermopower.

PACS numbers: 73.23.-b, 72.25.-b, 72.15.Qm, 73.50.Lw, 74.45.+c

I. INTRODUCTION

Systems containing quantum dots (QDs) or molecules coupled to different types of electrodes have been attracting non-decreasing attention for a few decades.^{1–4} As one of the most interesting phenomena in such systems the Kondo effect can be considered,⁵ in which the interaction with conduction electrons gives rise to many-body screening of the localized spin.⁶ This results in an additional resonance at the Fermi level in the local density of states and, consequently, to an enhanced conductance through the system for temperatures lower than the Kondo temperature T_K .^{7,8}

When the electron reservoirs, to which the dot is coupled, exhibit some correlations, the occurrence of the Kondo effect is conditioned by the ratio of T_K to the respective characteristic energy scale of correlated leads. In particular, in the case of superconducting electrodes, through multiple Andreev reflections at the quantum dot-superconductor interface, a Cooper pair carrying two electron charges can be transferred through the dot.^{9–12} In the Kondo regime this may lead to the conductance enhanced above the unitary limit $2e^2/h$, provided T_K is larger than the superconducting gap Δ .¹³ If, however, $\Delta > T_K$, the Kondo effect becomes suppressed and the conductance displays only small side resonances at energies corresponding to the energy gap.¹⁴ On the other hand, in the case of ferromagnetic leads, transport properties in the Kondo regime strongly depend on the relative orientation of the magnetizations of electrodes—the conductance usually drops when the magnetic configuration switches from the antiparallel into parallel one.^{15,16} This is related with an exchange field $\Delta\varepsilon_{\text{exch}}$ that emerges in the parallel configuration and acts in a similar way as an external magnetic field, splitting the dot level and

thus suppressing the linear conductance.^{15,17–19} It is thus the magnitude of the ferromagnetic-contact-induced exchange field that determines the emergence of the Kondo resonance in such systems.^{20–22}

For quantum dots coupled to both ferromagnetic and superconducting leads, transport properties are conditioned by a sensitive interplay of the exchange field, correlations leading to the Kondo effect and the superconductivity. Although transport through such hybrid devices in the Kondo regime has been recently experimentally measured,²³ theoretically this problem is still rather unexplored, although some considerations exist.^{24–33} These considerations, however, involved mainly the case of rather weak tunnel couplings between the dot and external leads, where the Kondo effect is not fully present and the effects due to the exchange field are not systematically included.

The goal of the present paper is therefore to provide a systematic and reliable analysis of transport properties of quantum dots with superconducting and ferromagnetic leads in the Kondo regime. To achieve this goal, we employ the full density-matrix numerical renormalization group (fDM-NRG) method,^{34–37} which allows for calculating various linear response transport coefficients in an accurate way. In particular we focus on the role of Andreev reflection in transport through a quantum dot coupled to the left and right ferromagnetic leads in a proximity with the third superconducting lead. We show that the exchange field due to ferromagnetic leads becomes modified by the coupling to the superconductor and is determined by the Andreev bound state energies. This fact is correspondingly reflected in the dependence of the dot's spectral function and the linear conductance on the dot level position and temperature. Moreover, we demonstrate that the effects due to the

proximity with the superconductor can be also resolved in thermoelectric transport properties. Thermoelectricity in confined nanostructures, such as quantum dots or molecules, has recently attracted a lot of attention due to relatively large values of the figure of merit,³⁸ which makes such nanoscale objects interesting for possible future applications.³⁹ Besides applicatory aspects, it turns out that measuring temperature dependence of the thermopower may provide additional information about (Kondo) correlations in the system.⁴⁰ Recently, the Seebeck and spin Seebeck coefficients in Kondo-correlated quantum dots were studied for nonmagnetic and ferromagnetic leads.^{40–43} Here, we will extend these studies to hybrid quantum dots with superconducting and ferromagnetic electrodes. To determine the thermopower in these hybrid devices, we assume that there is a temperature gradient between the ferromagnetic leads and analyze how the proximity effect influences the heat conductance and (spin) thermopower of the considered system in the Kondo regime.

The paper is organized as follows. In Sec. II we present the theoretical framework for our calculations. The model, relevant transport coefficients and method used in calculations are described therein. In Sec. III the numerical results on the dot's spectral function are presented and the analytical formula for the exchange field is derived. Section IV is devoted to the discussion of the linear conductance and tunnel magnetoresistance of the system, while in Sec. V we analyze the thermoelectric transport properties for different coupling strengths to the superconductor. Finally, the concluding remarks are given in Sec. VI.

II. THEORETICAL FRAMEWORK

A. Model

We consider a single-level quantum dot coupled to two ferromagnetic leads whose magnetizations can form either parallel (P) or antiparallel (AP) magnetic configuration, see Fig. 1. There is a temperature gradient δT applied between the ferromagnetic leads and the dot is additionally coupled to a superconducting lead. The Hamiltonian of the system is given by

$$H = H_{\text{QD}} + H_{\text{F}} + H_{\text{S}} + H_{\text{TF}} + H_{\text{TS}}, \quad (1)$$

where $H_{\text{QD}} = \sum_{\sigma} \varepsilon d_{\sigma}^{\dagger} d_{\sigma} + U d_{\uparrow}^{\dagger} d_{\downarrow}^{\dagger} d_{\downarrow} d_{\uparrow}$ describes the quantum dot, with d_{σ}^{\dagger} being the creation operator of an electron with spin σ and energy ε in the dot and U denoting the Coulomb correlations. The ferromagnetic leads are modeled within the noninteracting quasiparticle approximation, $H_{\text{F}} = \sum_{\alpha\mathbf{k}\sigma} \varepsilon_{\alpha\mathbf{k}\sigma} c_{\alpha\mathbf{k}\sigma}^{\dagger} c_{\alpha\mathbf{k}\sigma}$, where $\alpha = L$ ($\alpha = R$) for the left (right) lead and $c_{\alpha\mathbf{k}\sigma}^{\dagger}$ creates an electron of spin σ and momentum \mathbf{k} in lead α with the corresponding energy $\varepsilon_{\alpha\mathbf{k}\sigma}$. The s-wave superconductor is described by, $H_{\text{S}} = \sum_{\mathbf{k}\sigma} \xi_{\mathbf{k}\sigma} a_{\mathbf{k}\sigma}^{\dagger} a_{\mathbf{k}\sigma} - \Delta \sum_{\mathbf{k}} (a_{\mathbf{k}\uparrow}^{\dagger} a_{-\mathbf{k}\downarrow}^{\dagger} + a_{-\mathbf{k}\downarrow} a_{\mathbf{k}\uparrow})$,

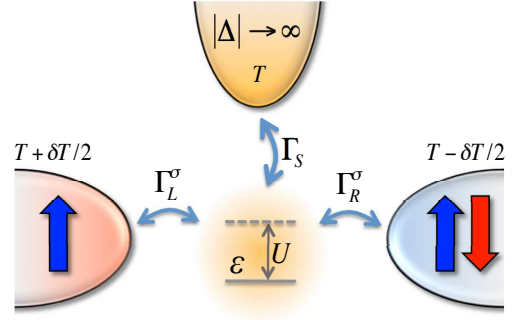


Figure 1. (color confine) Schematic of the considered system. Quantum dot, with dot level energy ε and Coulomb correlation U , is connected to two ferromagnetic and one superconducting lead. Γ_L^{σ} (Γ_R^{σ}) describes the spin-dependent coupling between the dot and the left (right) ferromagnetic lead and Γ_S is the coupling to the superconductor. The magnetizations of ferromagnets can form either parallel or antiparallel magnetic configuration, as indicated. There is a temperature gradient δT applied between the two ferromagnetic leads.

where $\xi_{\mathbf{k}\sigma}$ denotes the relevant single-particle energy, $a_{\mathbf{k}\sigma}^{\dagger}$ is the corresponding creation operator and Δ is the superconducting order parameter, which is assumed to be real and positive.

Finally, the last two terms of the Hamiltonian (1) describe tunneling processes between the dot and ferromagnetic and superconducting leads. They are respectively given by

$$H_{\text{TF}} = \sum_{\alpha=L,R} \sum_{\mathbf{k}\sigma} V_{\alpha\mathbf{k}\sigma} \left(d_{\sigma}^{\dagger} c_{\alpha\mathbf{k}\sigma} + c_{\alpha\mathbf{k}\sigma}^{\dagger} d_{\sigma} \right), \quad (2)$$

$$H_{\text{TS}} = \sum_{\mathbf{k}\sigma} V_{S\mathbf{k}\sigma} \left(d_{\sigma}^{\dagger} a_{\mathbf{k}\sigma} + a_{\mathbf{k}\sigma}^{\dagger} d_{\sigma} \right), \quad (3)$$

where $V_{\alpha\mathbf{k}\sigma}$ denotes the tunnel matrix elements between the dot and ferromagnetic leads, while $V_{S\mathbf{k}\sigma}$ is the tunnel matrix element between superconducting electrode and the dot. The strength of the coupling to ferromagnetic lead α for spin σ is given by $\Gamma_{\alpha}^{\sigma} = (1 + \sigma p_{\alpha})\Gamma$, where p_{α} is the spin polarization of ferromagnetic lead α , $p_{\alpha} = (\Gamma_{\alpha}^{\uparrow} - \Gamma_{\alpha}^{\downarrow})/(\Gamma_{\alpha}^{\uparrow} + \Gamma_{\alpha}^{\downarrow})$, and $\Gamma = \Gamma_L + \Gamma_R$, with $\Gamma_{\alpha} = (\Gamma_{\alpha}^{\uparrow} + \Gamma_{\alpha}^{\downarrow})/2$ and $\Gamma_{\alpha}^{\sigma} = \pi \rho_{\alpha}^{\sigma} V_{\alpha\sigma}^2$. Here, ρ_{α}^{σ} is the spin-dependent density of states of lead α and we assumed momentum independent matrix elements $V_{\alpha\mathbf{k}\sigma} \equiv V_{\alpha\sigma}$. In the following we also assume that the system is symmetric, $p_L = p_R \equiv p$ and $\Gamma_L = \Gamma_R \equiv \Gamma/2$. On the other hand, the coupling between the dot and the superconductor is given by, $\Gamma_S = \pi \rho_S V_S^2$, where ρ_S is the density of states of the superconductor in the normal state and we assumed momentum and spin independent tunnel matrix elements $V_{S\mathbf{k}\sigma} \equiv V_S$.

In this paper we focus on the linear-response spin-dependent transport properties of quantum dots in the proximity with the superconductor. We assume that the superconducting gap is larger than the corresponding charging energy of the dot. It implies that at low temperatures the only processes between the dot and supercon-

ducting lead are due to the Andreev reflection. We note that the charging energy in typical quantum dots can range from fractions of meV up to a few meV, while the superconducting energy gap can be as large as a couple of meV.^{44,45} Consequently, there are systems where the condition $U < \Delta$ is fulfilled. Aiming to focus on transport between the two ferromagnets, we set the electrochemical potential of the superconducting lead to zero and assume a small symmetric bias between ferromagnetic electrodes. Then, for symmetric couplings, the net current between the dot and the superconductor vanishes. In the limit of large Δ , the quantum dot with superconducting lead can be modeled by the following effective Hamiltonian^{46–48}

$$H_{\text{QD}}^{\text{eff}} = H_{\text{QD}} + \Gamma_S (d_{\uparrow}^{\dagger} d_{\downarrow}^{\dagger} + d_{\downarrow} d_{\uparrow}). \quad (4)$$

In this Hamiltonian the superconducting degrees of freedom have been integrated out and the possibility of creating or annihilating Cooper pairs in the superconductor is now included in the last, particle-non-conserving term proportional to Γ_S . This effective Hamiltonian can be easily diagonalized and has the following eigenstates: singly occupied dot states, $|\uparrow\rangle$ and $|\downarrow\rangle$, with energy ε and the two states being combinations of empty ($|0\rangle$) and doubly occupied ($|\uparrow\downarrow\rangle$) dot states

$$|\pm\rangle = \alpha_{\mp}|0\rangle \pm \alpha_{\pm}|\uparrow\downarrow\rangle, \quad (5)$$

with the coefficients, $\alpha_{\pm} = \sqrt{1 \pm \delta/(\delta^2 + \Gamma_S^2)}/\sqrt{2}$, and $\delta = \varepsilon + U/2$ denoting the detuning of the dot level from the particle-hole symmetry point $\varepsilon = -U/2$. The eigenenergies of the above eigenstates are given by, $E_{\pm} = \delta \pm \sqrt{\delta^2 + \Gamma_S^2}$, correspondingly. The excitation energies of the effective Hamiltonian (4) result in the following Andreev bound state energies

$$E_{\gamma\eta}^A = \gamma \frac{U}{2} + \eta \sqrt{\delta^2 + \Gamma_S^2}, \quad (6)$$

with $\gamma, \eta = \pm$. They correspond to respective excitations between the doublet and singlet states of the dot.

B. Transport coefficients

All the relevant linear-response transport coefficients can be expressed in terms of the following integral

$$L_{n\sigma} = -\frac{1}{h} \int d\omega \, \omega^n \frac{\partial f(\omega)}{\partial \omega} T_{\sigma}(\omega), \quad (7)$$

where $f(\omega)$ is the Fermi-Dirac distribution function and $T_{\sigma}(\omega)$ denotes the transmission coefficient. The spin-resolved linear conductance is then given by

$$G_{\sigma} = e^2 L_{0\sigma}. \quad (8)$$

In the case of ferromagnetic leads, depending on the spin relaxation time in ferromagnets, the voltage drop induced by temperature gradient can become spin dependent giving rise to spin accumulation, $\delta V_{\sigma} = \delta V + \sigma V_S$,

where V_S is the spin voltage. One can thus generally distinguish two different situations: (i) the first one when the spin relaxation is fast enough to assure $V_S = 0$ and (ii) the second one when spin relaxation is slow and $V_S \neq 0$. Moreover, in the three-terminal setup considered here, one needs to be careful about the current which can flow to the superconducting lead.³¹ To prevent the average current from flowing into the superconductor, we apply the temperature gradient δT symmetrically (see Fig. 1) and assume that the voltage guaranteeing the absence of the current J induced by temperature gradient is also applied symmetrically, that is $\mu_l = -\mu_r = \delta V/2$ and $\mu_S = 0$. Consequently, in the absence of spin accumulation, $V_S = 0$, the thermal conductance is given by

$$\kappa \equiv \left(\frac{\delta J_Q}{\delta T} \right)_{J=0} = \frac{1}{T} \left[L_2 - \frac{L_1^2}{L_0} \right], \quad (9)$$

where $L_n = \sum_{\sigma} L_{n\sigma}$. On the other hand, the Seebeck coefficient is defined as

$$S \equiv - \left(\frac{\delta V}{\delta T} \right)_{J=0} = - \frac{1}{|e|T} \frac{L_1}{L_0}. \quad (10)$$

The spin-dependent thermopower in the case of finite spin accumulation, $V_S \neq 0$ is defined by

$$S_{\sigma} \equiv - \left(\frac{\delta V_{\sigma}}{\delta T} \right)_{J_{\sigma}=0} = - \frac{1}{|e|T} \frac{L_{1\sigma}}{L_{0\sigma}}, \quad (11)$$

where J_{σ} denotes the current flowing in the spin channel σ . One can then define the thermopower and the spin thermopower as

$$S_{ac} = \frac{1}{2} (S_{\uparrow} + S_{\downarrow}), \quad (12)$$

$$S_S = \frac{1}{2} (S_{\uparrow} - S_{\downarrow}). \quad (13)$$

C. Method

To obtain reliable, experimentally testable predictions for transport properties of correlated quantum dots with ferromagnetic leads in the proximity with the superconductor, we employ the full density matrix numerical renormalization group method.^{34–37} This method allows us to study the dot's local density of states (dot-level spectral function) as well as the electric and thermoelectric transport properties in the full range of parameters in a very accurate way. In NRG, the conduction band is discretized logarithmically and the Hamiltonian is mapped onto a tight binding chain with exponentially decaying hoppings, which can be then diagonalized iteratively. In our calculations we kept 1024 states per iteration and used the Abelian symmetry for the total spin z th component.

To perform the analysis, we first applied an orthogonal left-right transformation to map the effective two-lead Hamiltonian to a new Hamiltonian, in which the dot

couples only to an even linear combination of electron operators of the left and right leads, with a new coupling strength $\Gamma = \Gamma_L + \Gamma_R$. We note that for left-right symmetric systems, such as considered in this paper, in the antiparallel configuration the effective coupling is the same for spin-up and spin-down electrons. As a result, transport characteristics are then qualitatively similar to those observed for nonmagnetic systems, except for a polarization dependent factor. In the parallel configuration, on the other hand, the effective couplings do depend on spin polarization of ferromagnets, giving rise to various interesting effects.

The main quantity we are interested in is the spin-dependent transmission coefficient

$$T_\sigma(\omega) = \frac{4\Gamma_L^\sigma \Gamma_R^\sigma}{\Gamma_L^\sigma + \Gamma_R^\sigma} \pi A_\sigma(\omega), \quad (14)$$

with $A_\sigma(\omega)$ being the spin-dependent spectral function of the dot, $A_\sigma(\omega) = -\frac{1}{\pi} \text{Im} G_\sigma^R(\omega)$, where $G_\sigma^R(\omega)$ is the Fourier transform of the retarded Green's function of the quantum dot for spin σ . In the parallel and antiparallel magnetic configurations the spin-resolved transmission coefficient acquires relatively simple form

$$T_\sigma^P(\omega) = (1 + \sigma p) \pi \Gamma A_\sigma^P(\omega), \quad (15)$$

$$T_\sigma^A(\omega) = (1 - p^2) \pi \Gamma A_\sigma^A(\omega), \quad (16)$$

respectively. Having determined the transmission, $T_\sigma(\omega)$, one can then calculate the integrals $L_{n\sigma}$, Eq. (7), and find the respective electric and thermoelectric transport coefficients. However, since in NRG one usually collects the spectral data in logarithmic bins that are then broadened to obtain a smooth curve, which may introduce some errors, we determine the transport coefficients directly from the discrete, high-quality NRG data.^{41,42} Nevertheless, when discussing the behavior of the dot spectral function, to improve its quality and suppress possible broadening artifacts,⁵⁰ in calculations we employ the z-averaging trick with the number of twist parameters $N_z = 5$.⁵¹

III. LOCAL DENSITY OF STATES AND EXCHANGE FIELD

A. Antiparallel configuration

The normalized spectral function in the antiparallel configuration, $\mathcal{A}^{\text{AP}}(\omega) = \sum_\sigma \pi \Gamma_\sigma^{\text{AP}} A_\sigma^{\text{AP}}(\omega)$, is shown in Fig. 2 for different couplings to the superconductor Γ_S . As mentioned above, in the antiparallel configuration the effective couplings $\Gamma_\sigma^{\text{AP}}$ become spin-independent and the system behaves as if coupled to nonmagnetic leads. Consequently, for $\Gamma_S = 0$, the spectral function exhibits the full Kondo resonance at $\omega = 0$. The Kondo temperature for the assumed parameters and for $\Gamma_S = 0$ is, $T_K/U \simeq 1.8 \times 10^{-3}$. There are also two Hubbard resonances, which for $\delta = 0$ occur at energies $\omega = \pm U/2$ (note

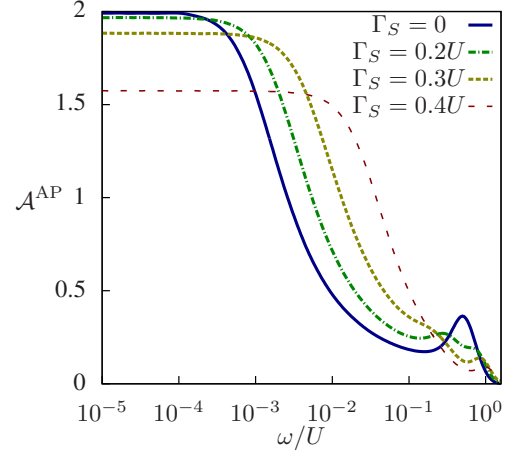


Figure 2. (color online) The energy dependence of the normalized spectral function in the antiparallel magnetic configuration \mathcal{A}^{AP} calculated for $\delta = 0$ and different couplings to superconducting lead Γ_S . The parameters are: $U = 1$, $\Gamma = U/12$, $T = 0$ and $p = 0.4$.

the logarithmic scale in Fig. 2). The proximity of superconducting lead results in gradual suppression of the Kondo effect with increasing Γ_S . For finite Γ_S , the virtual states for the spin-flip cotunneling processes driving the Kondo effect are the states $|+\rangle$ and $|-\rangle$, the energy of which greatly depends on Γ_S . This leads to a strong dependence of the Kondo temperature on the coupling to the superconductor. As can be seen in Fig. 2, increasing Γ_S generally raises the Kondo temperature. Moreover, for finite Γ_S , one can also observe two resonances for larger ω , which correspond to Andreev bound states of energies E_{++}^A and E_{+-}^A , see Fig. 2 for e.g. $\Gamma_S/U = 0.2$. When the coupling to the superconductor increases, the energies of the bound states change and, for larger Γ_S , the resonance at $\omega = E_{+-}^A$ merges with the Kondo peak, see the curve for $\Gamma_S/U = 0.4$ in Fig. 2.

The increase of the Kondo temperature for finite Γ_S is due to the fact that the excitation energies from the doublet state to singlet states $|+\rangle$ and $|-\rangle$ become decreased. As a consequence, an effective exchange interaction between the spin in the dot and the conduction electrons becomes enhanced with increasing Γ_S .

Another interesting feature visible in Fig. 2 is the decrease of the spectral function at the Fermi level with increasing Γ_S . In the case of $\Gamma_S = 0$, by the Friedel sum rule,^{6,52} the spectral function $A_\sigma(0)$ at $\omega = 0$ is given by, $A_\sigma(0) = (\pi\Gamma)^{-1}$, with $\Gamma_\uparrow = \Gamma_\downarrow \equiv \Gamma$. To understand the behavior of the spectral function in the presence of superconducting lead, let us have a look at the Green's function $\langle\langle d_\sigma | d_\sigma^\dagger \rangle\rangle_\omega$ of the dot-level, which in the wide band approximation is given by

$$\langle\langle d_\sigma | d_\sigma^\dagger \rangle\rangle_\omega = \left[\omega - \varepsilon - \Sigma_\sigma + i\Gamma - \frac{\Gamma_S^2}{\omega + \varepsilon + \Sigma_\sigma^S + i\Gamma} \right]^{-1}, \quad (17)$$

where the self-energies are defined as

$$\Sigma_\sigma = U \frac{\langle\langle d_\sigma n_{\bar{\sigma}} | d_\sigma^\dagger \rangle\rangle}{\langle\langle d_\sigma | d_\sigma^\dagger \rangle\rangle} \quad \text{and} \quad \Sigma_\sigma^S = U \frac{\langle\langle d_\sigma^\dagger n_{\bar{\sigma}} | d_\sigma^\dagger \rangle\rangle}{\langle\langle d_\sigma^\dagger | d_\sigma^\dagger \rangle\rangle}.$$

For the noninteracting case $U = 0$, and for $\varepsilon = 0$, the spectral function at $\omega = 0$ is $A_\sigma(0) = (\pi\tilde{\Gamma})^{-1}$, with

$$\tilde{\Gamma} = \Gamma \left(1 + \frac{\Gamma_S^2}{\Gamma^2} \right). \quad (18)$$

Clearly, the height of the spectral function at the Fermi level decreases with increasing Γ_S . The same tendency also holds for the fully interacting case, see Fig. 2, the decrease in $A_\sigma(0)$ is however smaller than in the noninteracting case, since the denominator in Eq. (18) is larger due to finite self-energy Σ_σ^S , see Eq. (17). Note that for $\varepsilon = -U/2$ (the particle-hole symmetry point of the Anderson model), $\text{Re}\{\Sigma_\sigma^S(\omega = 0)\} \neq U/2$, contrary to the self-energy Σ_σ , which then fulfills $\text{Re}\{\Sigma_\sigma(\omega = 0)\} = U/2$.

B. Parallel configuration

Figure 3 presents the energy and level detuning dependence of the normalized spectral function in the parallel magnetic configuration, $\mathcal{A}^P(\omega) = \sum_\sigma \pi \Gamma_\sigma^P A_\sigma^P(\omega)$. $\mathcal{A}^P(\omega)$ is calculated for a few different values of the coupling to the superconductor Γ_S , as indicated in the figure. By changing the level detuning δ , the occupancy of the dot changes. For $|\delta| < \sqrt{U^2/4 - \Gamma_S^2}$, the dot is singly occupied, while for $|\delta| > \sqrt{U^2/4 - \Gamma_S^2}$, the occupancy is even, i.e. the dot is in state $|+\rangle$ for $\delta < -\sqrt{U^2/4 - \Gamma_S^2}$, and in state $|-\rangle$ for $\delta > \sqrt{U^2/4 - \Gamma_S^2}$.

In the singly occupied regime, for $T < T_K$, the electronic correlations may give rise to a resonance at the Fermi level due to the Kondo effect. This is indeed what one observes for the antiparallel magnetic configuration, see Fig. 2. However, due to the dependence of tunneling processes on spin, in the parallel configuration the dot levels for spin-up and spin-down become renormalized and shift in opposite directions, leading to a spin splitting of the dot level, $\Delta\varepsilon_{\text{exch}}$. This exchange field created by the presence of ferromagnetic leads suppresses the Kondo effect once $|\Delta\varepsilon_{\text{exch}}| > T_K$. Moreover, $\Delta\varepsilon_{\text{exch}}$ displays a particular dependence on the level detuning δ , it vanishes for $\delta = 0$ and changes sign at the particle-hole symmetry point. Although by splitting the dot level the exchange field acts in a similar way as an external magnetic field, it possesses an extra asset, namely that its magnitude and sign can be tuned by purely electrical means, i.e. by changing δ with a gate voltage.

All the above-mentioned features can be clearly visible in Fig. 3(a), which presents the spectral function for $\Gamma_S = 0$. Firstly, the zero-energy spectral function $\mathcal{A}^P(0)$ has two maxima broadened by 2Γ at resonant energies $\delta = \pm U/2$. Secondly, in the singly occupied dot regime, one observes the Kondo resonance for $\delta = 0$, which then

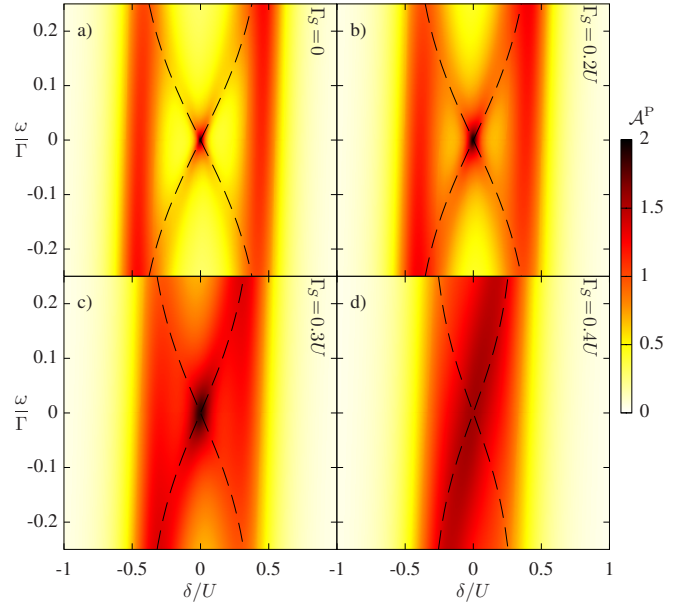


Figure 3. (color online) The normalized spectral function \mathcal{A}^P in the parallel magnetic configuration as a function of energy ω and level detuning $\delta = \varepsilon + U/2$ for different couplings to superconducting lead: (a) $\Gamma_S = 0$, (b) $\Gamma_S/U = 0.2$, (c) $\Gamma_S/U = 0.3$, (d) $\Gamma_S/U = 0.4$. The dashed lines show the exchange field $\Delta\varepsilon_{\text{exch}}$ obtained from the analytical formula (20). The parameters are the same as in Fig. 2.

becomes split as the level detuning increases, $|\delta| > 0$. The split Kondo resonance due to the presence of ferromagnetic leads has already been observed in a number of experiments and is rather well understood.^{15–22} Here, we in particular want to analyze how the superconducting proximity effect affects the exchange field and, thus, the split Kondo resonance. For finite Γ_S , the resonant energies are $\delta = \pm\sqrt{U^2/4 - \Gamma_S^2}$. This implies that the singly occupied regime shrinks with increasing the coupling to the superconductor. Consequently, the Kondo temperature increases, since the excitation energies from singly occupied to evenly occupied virtual states, $|+\rangle$ and $|-\rangle$, become lowered. Moreover, the magnitude of the exchange field also becomes enhanced with increasing Γ_S . However, while the increase of $\Delta\varepsilon_{\text{exch}}$ with Γ_S is algebraic, the T_K -dependence on Γ_S is rather exponential. Therefore, for large Γ_S , the effects due to the proximity with ferromagnets become eventually overwhelmed by the Kondo correlations. This is visible in Fig. 3, where the width of the split Kondo resonances become increased, till they eventually merge for large Γ_S , see Fig. 3(d). In fact, for $\Gamma_S = 0.4U$, the local moment regime of the dot is relatively narrow and due to the broadening of the resonant peaks, one observes only a single low-energy resonance for $\delta = 0$. The height of this resonance is however lower as compared to the case of smaller Γ_S , which indicates that although the strong coupling to the superconductor can suppress the effects due to the exchange field, it may also destroy the Kondo

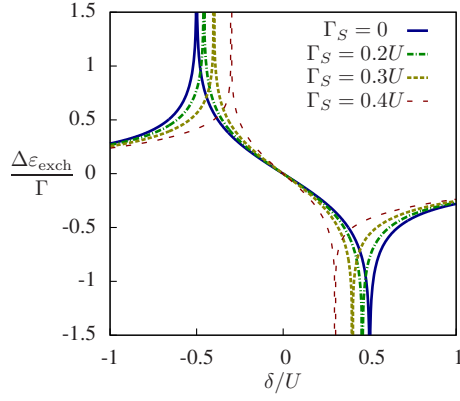


Figure 4. (color online) The exchange field in the parallel magnetic configuration for a few values of Γ_S obtained from Eq. (20) at $T = 0$. The other parameters are as in Fig. 2.

effect.

C. Perturbative analysis

To estimate the magnitude of the exchange field in the parallel configuration in the presence of the superconductor, one can use the second-order perturbation theory to determine the spin-dependent dot level renormalization $\delta\varepsilon_\sigma$ due to the coupling to ferromagnets. We thus treat H_{TF} as a perturbation to $H_0 = H_{\text{QD}}^{\text{eff}} + H_F$, and find that the shift of the level is given by

$$\delta\varepsilon_\sigma = -\frac{\Gamma_\sigma}{\pi} \int d\omega \left[\frac{\alpha_+^2 f^-(\omega)}{\omega - E_{-+}^A} + \frac{\alpha_-^2 f^-(\omega)}{\omega - E_{--}^A} \right] - \frac{\Gamma_{\bar{\sigma}}}{\pi} \int d\omega \left[\frac{\alpha_+^2 f(\omega)}{\omega - E_{++}^A} + \frac{\alpha_-^2 f(\omega)}{\omega - E_{+-}^A} \right], \quad (19)$$

where $f^-(\omega) = 1 - f(\omega)$. The exchange field can be then obtained from $\Delta\varepsilon_{\text{exch}} = \delta\varepsilon_\uparrow - \delta\varepsilon_\downarrow$ and is given by

$$\Delta\varepsilon_{\text{exch}} = \frac{2p\Gamma}{\pi} \frac{\delta}{\sqrt{\delta^2 + \Gamma_S^2}} [\phi(E_{+-}^A) - \phi(E_{++}^A)], \quad (20)$$

where $\phi(\omega) = \text{Re} \left\{ \Psi \left(\frac{1}{2} + i \frac{\omega}{2\pi T} \right) \right\}$ and $\Psi(z)$ is the digamma function. Clearly, the exchange field is a function of the Andreev bound state energies and can be tuned not only by δ , but also by Γ_S . Although $\Delta\varepsilon_{\text{exch}}$ results directly from the proximity effect with the ferromagnetic leads, the superconducting proximity effect may considerably affect it. The formula for the exchange field, Eq. (20), can be somewhat simplified at zero temperature when, $\phi(E_{+-}^A) - \phi(E_{++}^A) = \log |E_{+-}^A/E_{++}^A|$, while for $\Gamma_S = 0$, one gets,^{17,20–22} $\Delta\varepsilon_{\text{exch}} = \frac{2p\Gamma}{\pi} \log \left| \frac{\delta - U/2}{\delta + U/2} \right|$.

The exchange field obtained from Eq. (20) as a function of level detuning δ is plotted in Fig. 4. The perturbation theory breaks down at resonances, for $|\delta| = \sqrt{U^2/4 - \Gamma_S^2}$, where the exchange field diverges at $T = 0$. We plotted

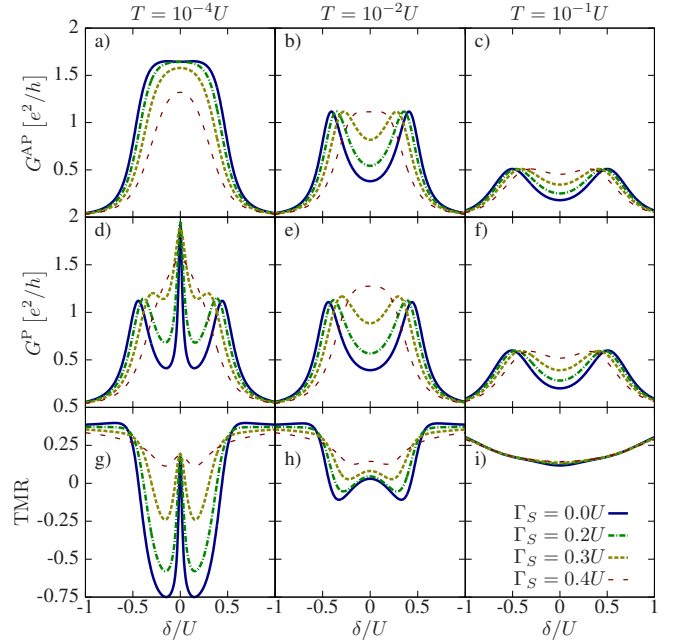


Figure 5. (color online) The level detuning dependence of the linear conductance in the antiparallel G^{AP} (a)-(c) and parallel G^{P} (d)-(f) magnetic configurations as well as the resulting TMR (g)-(i) for different couplings to the superconductor and temperatures. The left, middle and right columns correspond to $T/U = 10^{-4}$, $T/U = 10^{-2}$ and $T/U = 10^{-1}$, respectively. The other parameters are as in Fig. 2.

$\Delta\varepsilon_{\text{exch}}$ in the full range of δ to present how the resonances move towards the middle of the Coulomb blockade regime with increasing Γ_S . Another feature visible in Fig. 4 is the enhancement of the magnitude of the exchange field in the singly occupied dot regime with raising the coupling to the superconductor. $\Delta\varepsilon_{\text{exch}}$ obtained from formula (20) is also shown in Fig. 3 by dashed lines. One can see that the agreement between the split Kondo resonances visible in the spectral function obtained by NRG and the estimation for $\Delta\varepsilon_{\text{exch}}$ based on Eq. (20) is indeed very good. For large coupling to the superconductor, however, the spectral function displays only one broad Kondo resonance and the splitting is no longer visible due to the broadening of Andreev levels by the coupling to ferromagnetic leads Γ .

IV. LINEAR CONDUCTANCE AND TUNNEL MAGNETORESISTANCE

In this section we focus on the role of superconducting proximity effect on the spin-resolved electric transport coefficients. In particular, we study the level detuning and temperature dependence of the linear conductance in the parallel (G^{P}) and antiparallel (G^{AP}) magnetic configurations, as well as the resulting tunnel magnetoresistance, which is defined as,⁴⁹ $\text{TMR} = G^{\text{P}}/G^{\text{AP}} - 1$.

A. Level detuning dependence

In Fig. 5 we show the level detuning dependence of the linear conductance and the TMR for different temperatures and couplings to the superconductor. At low temperatures, $T < T_K$, in the antiparallel configuration there is a Kondo plateau in the singly occupied regime where $G^{\text{AP}} = 2(1-p^2)e^2/h$, see Fig. 5(a), which becomes suppressed with increasing Γ_S . At intermediate temperatures, $T/U = 10^{-2}$ [Fig. 5(b)], for $\Gamma_S = 0$, the Kondo effect is suppressed since $T > T_K$, however, by increasing the coupling to the superconductor, one also increases the Kondo temperature and for $\Gamma_S/U = 0.4$ there is a single resonance around $\delta = 0$. Note, however, that this maximum in G^{AP} is mainly due to the fact that the resonant energies become very close and the two resonant peaks merge due to the broadening of Andreev levels by the coupling to ferromagnetic leads. In the case of relatively high temperatures, $T/U = 10^{-1}$, the general dependence is similar to the previous case, but the conductance is suppressed.

In the parallel configuration, the linear conductance at low temperatures shows a clear signature of the exchange field that suppresses the Kondo effect for $\delta \neq 0$, while for $\delta = 0$ the conductance is maximum, $G^{\text{P}} = 2e^2/h$, see Fig. 5(d). With increasing Γ_S , the effects due to the exchange field are effectively decreased and almost completely disappear for $\Gamma_S/U = 0.4$, as explained in Sec. III. On the other hand, for higher temperatures, $|\Delta\varepsilon_{\text{exch}}| < T$, such that thermal fluctuations smear out the effects due to the exchange field, the dependence of G^{P} on δ is qualitatively similar to that for G^{AP} , with a general tendency that for $T \gtrsim \Gamma$, $G^{\text{P}} > G^{\text{AP}}$, compare Figs. 5(c) and (f).

The difference in G^{P} and G^{AP} gives rise to nonzero TMR presented in Figs. 5(g)-(i). While for $T < T_K$ and $\Gamma_S = 0$, the TMR exhibits a highly nontrivial dependence on level detuning δ ,²¹ with increasing either Γ_S or T , the TMR dependence on T becomes less dramatic. First of all, when raising Γ_S , the effects due to the exchange field become suppressed and the TMR becomes positive in the whole range of δ . Moreover, for larger temperatures, the proximity of the superconductor plays a smaller role and for $T/U = 10^{-1}$, see Fig. 5(i), the TMR is roughly independent of Γ_S .

B. Temperature dependence

The behavior described above is also visible in the temperature dependence of the linear conductance and TMR shown in Fig. 6, which is calculated for several values of δ and Γ_S . For the particle-hole symmetric case $\delta = 0$ presented in the left column of Fig. 6, both G^{P} and G^{AP} exhibit dependence on T , which is typical for quantum dots in the Kondo regime.²¹ They just differ by a polarization-dependent factor, which in the Kondo regime is equal to $1 - p^2$, and with increasing tempera-

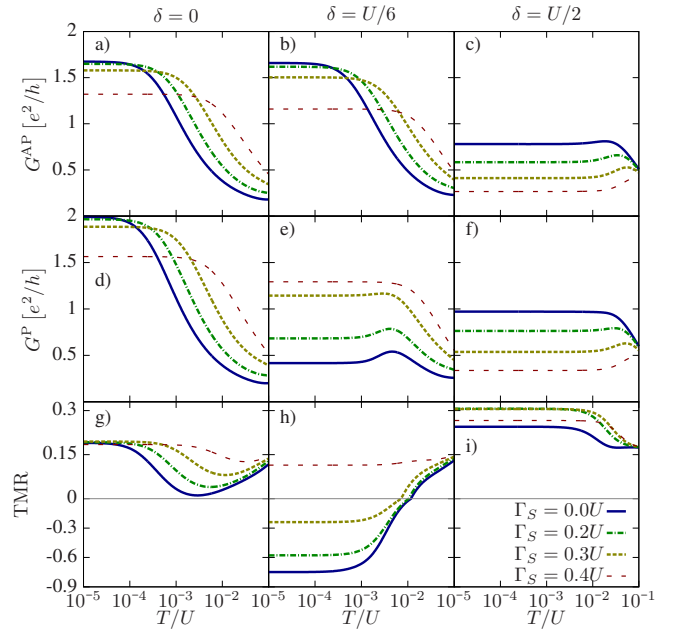


Figure 6. (color online) The temperature dependence of G^{AP} (a)-(c), G^{P} (d)-(f) and the TMR (g)-(i) for different couplings Γ_S . The left, middle and right columns correspond to $\delta = 0$, $\delta = U/6$ and $\delta = U/2$, respectively. The other parameters are the same as in Fig. 2.

ture becomes decreased for $T \approx T_K$ to raise again once thermally-activated sequential processes become possible. As a result, the TMR is given by, $\text{TMR} = p^2/(1-p^2)$, in the Kondo regime, $T < T_K$, and in the sequential tunneling regime, $T \gtrsim \Gamma$, and becomes suppressed for $T \approx T_K$, see Fig. 6(g). With increasing the coupling to the superconductor, these features basically persist, but the Kondo temperature becomes increased, see Figs. 6(a) and (d). In addition, one can observe that the height of the Kondo resonance is gradually suppressed with increasing Γ_S . This can be understood by realizing that the proximity of the superconductor effectively diminishes the repulsion of electrons in the dot. Since the Coulomb repulsion is necessary for the Kondo effect to occur, an increase of Γ_S will inevitably lead to the suppression of the Kondo resonance.

In the Coulomb blockade regime when the particle-hole symmetry is broken, the exchange field starts playing an important role. This situation is presented in the middle column of Fig. 6, which is calculated for $\delta = U/6$. While the temperature dependence of G^{AP} is very similar to the case of $\delta = 0$, see Figs. 6(a) and (b), the linear conductance in the parallel configuration is completely different. G^{P} is generally suppressed as compared to the particle-hole symmetric case, which is due to the presence of exchange field. The Kondo resonance is suppressed and the linear conductance in parallel configuration displays only a small maximum for temperatures of the order of the Kondo temperature, see Fig. 6(e). This results in highly nontrivial dependence of the TMR

on T [Fig. 6(h)], which now takes large negative values for $T < T_K$ and then becomes positive with increasing temperature. However, when the coupling to superconducting lead increases, there appears a competition between the exchange field and the superconducting proximity effect, so that the role of the exchange field becomes diminished, and the difference in conductances for both magnetic configurations is lowered, see Figs. 6(b) and (e). Consequently, for relatively strong coupling Γ_S , the TMR becomes positive in the whole range of temperatures, see the case of $\Gamma_S/U = 0.4$ in Fig. 6(h).

The right column of Fig. 6 presents the case when $\delta = U/2$, i.e. for $\Gamma_S = 0$ the system is on resonance. With increasing Γ_S , the resonance moves towards the middle of the Coulomb blockade and the dot becomes occupied by the state $|+\rangle$. This results in lowering of the linear conductance with increasing Γ_S , irrespective of the magnetic configuration of the system, see Figs. 6(c) and (f). In fact, when raising the coupling to the superconductor, the transport regime changes from resonant to cotunneling regime. As a consequence, the TMR increases with Γ_S to reach the value $\text{TMR} = 2p^2/(1-p^2)$, characteristic of non-spin-flip cotunneling regime.⁵³ However, for higher temperatures, $T \gtrsim \Gamma$, the thermally-activated sequential transport dominates and TMR becomes lowered, reaching $\text{TMR} = p^2/(1-p^2)$, see Fig. 6(i).

V. SEEBECK AND SPIN SEEBECK COEFFICIENTS

We now move to the discussion of thermoelectric transport properties of the system. For this, we assume that there is a temperature gradient δT applied to the left and right ferromagnetic leads, see Fig. 1. The formulas for the relevant thermoelectric coefficients are presented in Sec. II.B. First, we study the influence of the proximity effect on the thermoelectric coefficients in the case of no spin accumulation in the leads and then proceed to the case of finite spin accumulation and the analysis of the spin Seebeck effect.

A. Absence of spin accumulation in the leads

Before analyzing the behavior of the thermopower, in Fig. 7 we show the thermal conductance κ as a function of the level detuning δ for different temperatures and couplings to superconducting lead. The left column corresponds to the antiparallel configuration, while the right column shows the results in the parallel configuration. When decreasing temperature, the thermal conductance becomes generally suppressed, however, specific shape of its dependence on δ also changes. At high temperatures, $T/U = 0.1$, κ displays a maximum for $\delta = 0$, where the particle and hole processes equally contribute to transport. This is visible in both magnetic configurations, see Figs. 7(a) and (b), although κ is larger in the parallel

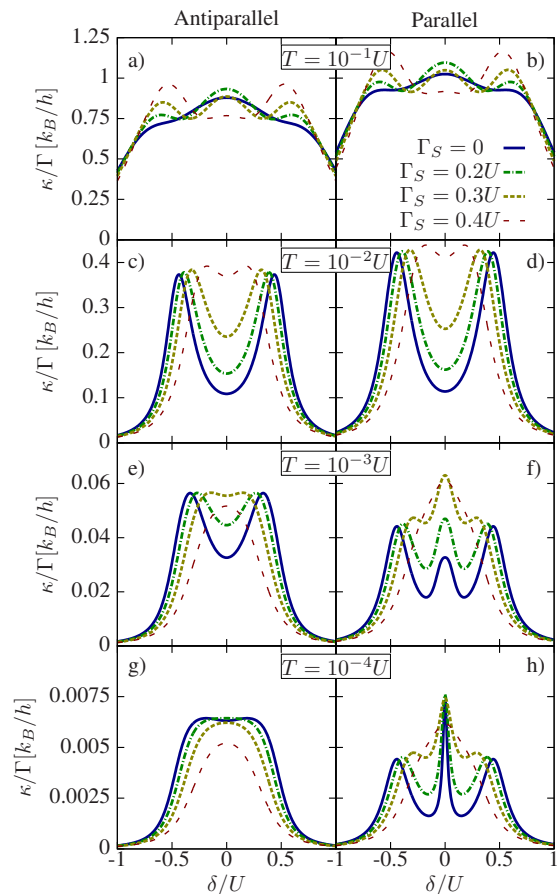


Figure 7. (color online) The thermal conductance κ as a function of detuning δ for the antiparallel (left column) and parallel (right column) configurations and for different couplings to the superconductor Γ_S . Each row corresponds to different temperature, as indicated. The parameters are the same as in Fig. 2.

configuration as compared to the antiparallel one. With increasing the coupling to the superconductor, the maximum changes into local minimum, while two maxima for $\delta \approx \pm U/2$ develop. For intermediate temperatures, $T/U = 0.01$, the shape of the δ -dependence of κ becomes similar to the detuning dependence of the linear conductance, cf. Fig. 5. Similar tendency can be also observed for lower temperatures, however, while the conductance increases with decreasing T , the thermal conductance becomes suppressed to disappear completely at zero temperature. Furthermore, at low temperatures, when $|\Delta\varepsilon_{\text{exch}}| \gtrsim T$, the exchange field starts playing an important role and the difference between both magnetic configurations becomes clearly visible. When raising Γ_S , the influence of the exchange field on transport becomes relatively weakened. The suppressed thermal conductance in the parallel configuration in the Coulomb blockade regime becomes then enhanced. On the other hand, in the antiparallel configuration, the Kondo effect becomes gradually destroyed and κ drops in the local

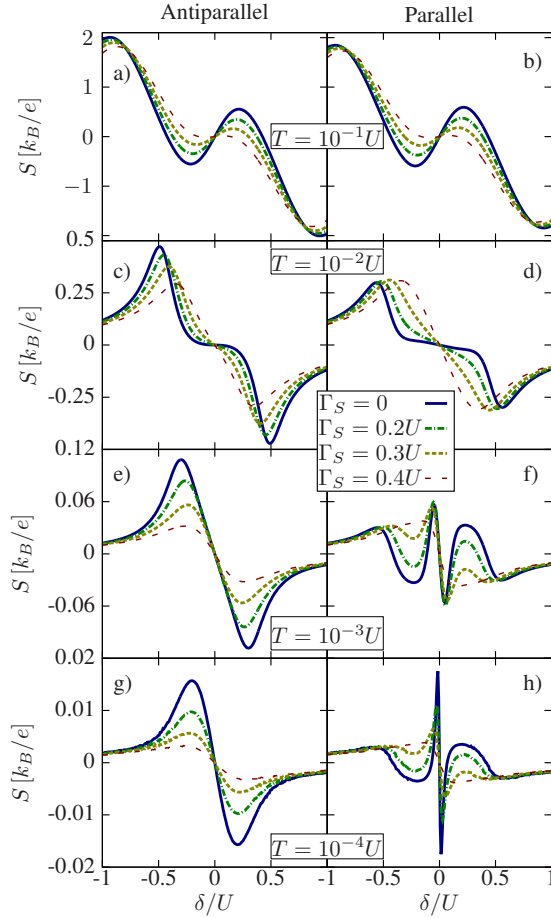


Figure 8. (color online) The thermopower as a function of δ for the antiparallel (left column) and parallel (right column) configurations and for different Γ_S and T , as indicated. The other parameters are as in Fig. 2.

moment regime with increasing Γ_S , see Figs. 7(g) and (h).

Figure 8 shows the δ -dependence of the Seebeck coefficient in both magnetic configurations for different temperatures and couplings Γ_S . The behavior of the thermopower is mostly determined by the shape of the Kondo peak in the local density of states. For $\delta = 0$, the Kondo resonance is fully symmetric around the Fermi level and, consequently, the particle and hole currents compensate each other and the thermopower vanishes. When moving away from the particle-hole symmetry point, the Seebeck coefficient becomes nonzero and its sign depends on the relative magnitude of the particle and hole currents. S is thus an odd function of δ . At higher temperatures, the behavior of S is qualitatively similar in both magnetic configurations, see Figs. 8(a) and (b). The thermopower has a local maximum (minimum) for $0 < \delta < U/2$ ($-U/2 > \delta > 0$). The differences between S in the parallel and antiparallel configuration start showing up with lowering temperature, when the exchange field starts playing a role. In the antiparallel configu-

ration, for $0 < \delta < U/2$, the local maximum in S for $T/U = 0.1$ gradually merges with a local minimum, the position of which moves from $\delta \approx U$ towards $\delta = 0$ with lowering temperature. When increasing the coupling to superconducting lead, the thermopower in the antiparallel configuration (and in the parallel configuration for $T > |\Delta\varepsilon_{\text{exch}}|$) becomes generally suppressed, however its qualitative dependence on δ remains the same. This is opposite to what we have in the parallel configuration, especially at low temperatures, when $T < |\Delta\varepsilon_{\text{exch}}|$, see Figs. 8(f) and (h). Then, for $0 < \delta < U/2$, S exhibits a local minimum, which becomes sharper and moves towards $\delta = 0$ with lowering T . With increasing δ , this minimum changes into a local maximum to drop again for $\delta \approx U/2$. As a consequence, for $\delta > 0$, S changes sign twice in the Coulomb blockade regime. This is related to the exchange field, which suppresses the Kondo resonance, once $|\Delta\varepsilon_{\text{exch}}| > T_K, T$. Since $\Delta\varepsilon_{\text{exch}}$ depends strongly on δ , it leads to the aforementioned behavior of the thermopower around the particle-hole symmetry point $\delta = 0$. Interestingly, when the coupling to the superconductor is increased, the δ -dependence of S changes drastically. In particular, for large Γ_S , when the exchange field effects are suppressed by superconducting proximity effect, the difference between the two magnetic configurations is decreased, and S in the parallel configuration behaves similarly to S in the antiparallel configuration. Altogether, this gives rise to a nontrivial dependence of the low-temperature thermopower on Γ_S in the parallel configuration. The interplay of the three relevant energy scales: superconducting gap, exchange field and Kondo temperature is then clearly revealed, see Fig. 8.

B. Finite spin accumulation in the leads

We now discuss the behavior of the spin thermopower in the parallel magnetic configuration in the case of finite spin accumulation in the leads. Such situation arises when the spin relaxation in the leads is slow and the shifts of the chemical potential for spin-up and spin-down electrons induced by the temperature gradient are not equal. The δ -dependence of the spin Seebeck coefficient is presented in Fig. 9 for different temperatures and couplings to the superconductor. For $T/U = 0.1$, the spin thermopower changes monotonically with sweeping δ from $-U$ to U , see Fig. 9(a). Finite coupling to the superconductor leads only to the suppression of S_S . For smaller temperatures, however, S_S exhibits a maximum (minimum) for $\delta > 0$ ($\delta < 0$), see the case of $T/U = 0.01$ in Fig. 9. This maximum is still present when the coupling to the superconductor becomes stronger, while its position moves towards the middle of the Coulomb blockade with increasing Γ_S . Moreover, for relatively strong coupling to the superconductor, $\Gamma_S/U = 0.4$, one can see that the δ -dependence of the spin thermopower has changed qualitatively. Now, S_S for $\delta > 0$ exhibits a

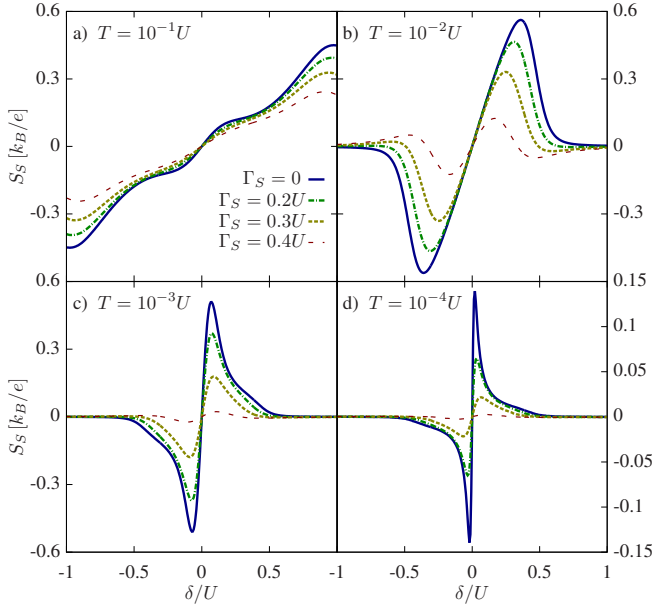


Figure 9. (color online) The spin thermopower in the parallel configuration as a function of δ for different Γ_S and for: (a) $T/U = 10^{-1}$, (b) $T/U = 10^{-2}$, (c) $T/U = 10^{-3}$ and (d) $T/U = 10^{-4}$. The other parameters are the same as in Fig. 2.

sign change in the Coulomb blockade regime, which was not present in the case of $\Gamma_S = 0$. When further decreasing the temperature, the maximum in S_S for positive detuning moves towards the particle-hole symmetry point $\delta = 0$ and its magnitude becomes suppressed, see Figs. 9(c) and (d). For given temperature, increasing the strength of the coupling to superconducting lead, results in a large suppression of the spin thermopower. The spin Seebeck coefficient for $T \lesssim T_K$ becomes almost fully suppressed in the case of strong coupling to the superconductor.

For completeness, in Fig. 10 we show the detuning dependence of the Seebeck coefficient for different temperatures and couplings Γ_S in the case of finite spin accumulation in the leads. Except for opposite sign, the dependence of S_{ac} on δ , T and Γ_S is quite similar to the dependence of the spin Seebeck coefficient, cf. Figs. 9 and 10, although some differences still appear. First of all, for temperatures considered in Fig. 10, S_{ac} exhibits a nonmonotonic dependence on δ , contrary to S_S , which for $T/U = 0.1$ changed rather monotonically. Moreover, the dependence on Γ_S for S_{ac} is now weaker as compared to S_S . Increasing the coupling to the superconductor results only in quantitative changes, leading generally to the suppression of the thermopower S_{ac} , see Fig. 10.

Finally, it is also interesting to study the temperature dependence of S_S and S_{ac} in the parallel configuration for different coupling Γ_S , see Fig. 11. The left (right) column corresponds to $\delta = U/6$ ($\delta = U/2$). Let us first consider the case of $\delta = U/6$, when the system is in the Coulomb blockade regime. For very high ($T > U$) or very low ($T < T_K$) temperatures, both S_S and S_{ac} tend to zero

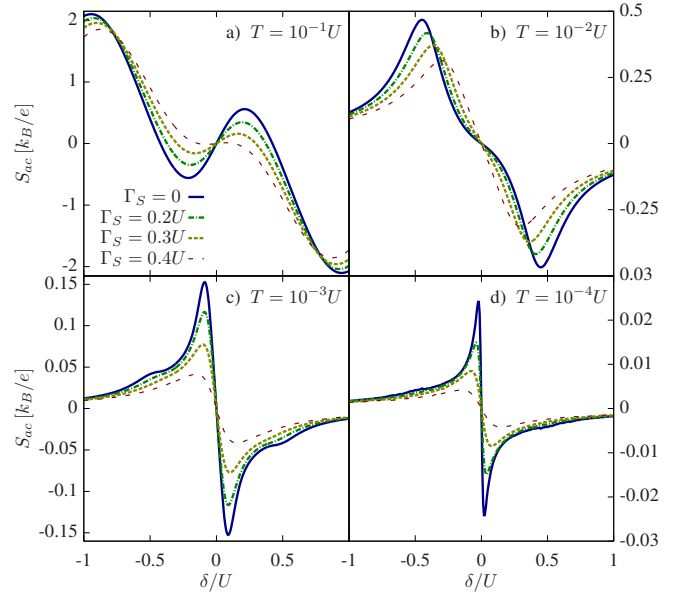


Figure 10. (color online) The thermopower in the parallel configuration as a function of δ for different Γ_S and for different temperatures in the case of finite spin accumulation. The parameters are the same as in Fig. 2.

for all values of Γ_S , see Figs. 11(a) and (c). However, for intermediate temperatures, $T \sim T_K$, the spin Seebeck coefficient exhibits a maximum, the height of which diminishes with increasing Γ_S . The temperature at which the maximum occurs increases when the coupling to the superconductor is stronger. In addition, for $\Gamma_S = 0$ there is also a small local maximum for $T \approx \Gamma$, which however merges with the large peak when Γ_S is increased, see Fig. 11(a). Contrary to S_S , the temperature dependence of S_{ac} reveals two sign changes. With increasing T , S_{ac} first drops to a local minimum for $T \sim T_K$, then changes sign and reaches a local maximum for $T \sim \Gamma$ to drop again for $T \sim U$ with another sign change, see Fig. 11(c). When increasing the coupling to the superconductor, the temperature at which the first minimum occurs increases, while the positions of other extrema are rather unchanged. Moreover, the overall magnitude of S_{ac} becomes generally suppressed with increasing Γ_S , which is especially visible for $T \sim \Gamma$, see Fig. 11(c).

For larger detuning, $\delta = U/2$, the system is on resonance for $\Gamma_S = 0$. The temperature dependence of the spin thermopower displays then a single maximum for temperatures of the order of the coupling Γ . With increasing the coupling to the superconductor, this maximum transforms into a local minimum and S_S exhibits a sign change when increasing temperature, see Fig. 11(b). This is opposite to S_{ac} , which is now negative in the whole range of temperatures, irrespective of Γ_S , see Fig. 11(d). The Seebeck coefficient has two local minima for $T \sim \Gamma$ and $T \sim U$, separated by a local maximum, which merge together with increasing Γ_S into a large single minimum for $T \sim \Gamma$. Consequently, the proximity of

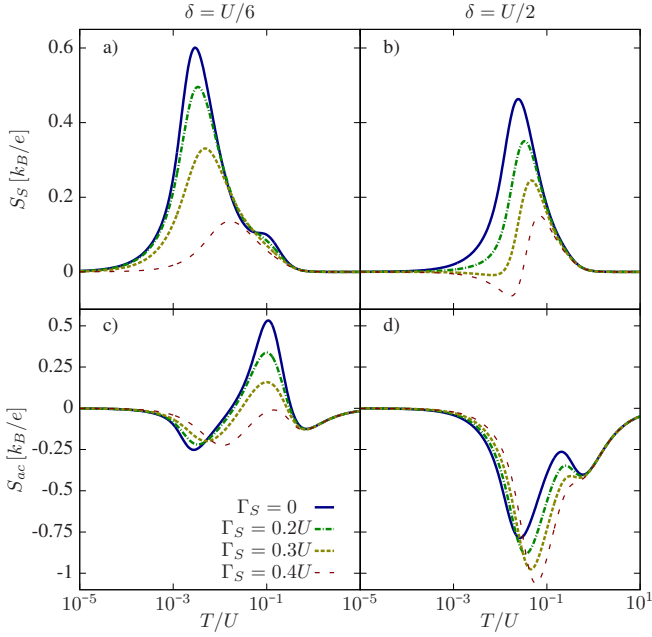


Figure 11. (color online) The spin thermopower (a,b) and thermopower (c,d) in the parallel configuration as a function of temperature for different Γ_S in the case of finite spin accumulation. The left column corresponds to $\delta = U/6$, while the right column to $\delta = U/2$. The parameters are as in Fig. 2.

the superconductor generally enhances the Seebeck coefficient S_{ac} . This behavior is opposite to that of S_S and S_{ac} in the case of $\delta = U/6$ discussed above, for which the proximity effect led to a general suppression of the (spin) thermopower.

Finally, we would like to note that although the range of temperatures studied in Fig. 11 may be slightly too large to assure that the description based on effective Hamiltonian in the limit of large superconducting gap is reasonable, we showed the data at high temperatures $T \gtrsim U$ for completeness and consistency. Nevertheless, the most interesting behavior of the Seebeck and spin Seebeck coefficients discussed above occurs in the temperature range where the assumptions used are correct.

VI. CONCLUDING REMARKS

In the present paper we analyzed the electric and thermoelectric transport properties of Kondo-correlated

quantum dots coupled to the left and right ferromagnetic leads and additionally coupled to one superconducting lead. In such hybrid devices, transport characteristics are determined by the interplay of ferromagnetic-contact induced exchange field, the superconducting proximity effect and correlations leading to the Kondo effect. By using the full density-matrix numerical renormalization group method, we determined the dot's spectral function, linear electric and thermal conductances, the TMR and the (spin) Seebeck coefficient for different temperatures, level positions and couplings to the superconductor in the limit of large superconducting gap. We showed that the superconducting proximity effect may considerably affect the exchange field, which is a function of Andreev bound state energies. For the exchange field, we provided an approximative analytical formula that agrees well with the NRG calculations. The exchange field leads to a spin-splitting of the dot level, which can suppress the Kondo resonance. We demonstrated that increasing the coupling to the superconductor may raise the Kondo temperature and partially restore the exchange-field-split Kondo resonance. This subtle competition between ferromagnetic and superconducting proximity effects is clearly visible in the corresponding temperature and level detuning dependence of both the electric and thermoelectric transport coefficients of the system.

ACKNOWLEDGMENTS

The discussions with J. Barnaś, K. Bocian, W. Rudziński and P. Trocha are gratefully acknowledged. We also thank J. Barnaś and P. Trocha for critical reading of this manuscript. This work is supported by the 'Iuventus Plus' project No. IP2011 059471 for years 2012-2014 and the National Science Center in Poland as the Project No. DEC-2012/04/A/ST3/00372. This research was also supported by a Marie Curie FP-7-Reintegration-Grants (grant No. CIG-303 689) within the 7th European Community Framework Programme.

* kpwojcik@amu.edu.pl

† weymann@amu.edu.pl

¹ *Single Charge Tunneling: Coulomb Blockade Phenomena in Nanostructures*, NATO ASI Series B: Physics 294, ed. by H. Grabert, M.H. Devoret (Plenum Press, New York 1992).

² *Mesoscopic Electron Transport*, ed. by L.L. Sohn,

L.P. Kouwenhoven, G. Schön (Kluwer, Dordrecht 1997).

³ *Semiconductor Spintronics and Quantum Computation*, ed. by D.D. Awschalom, D. Loss, and N. Samarth (Springer, Berlin 2002).

⁴ S. Andergassen, V. Meden, H. Schoeller, J. Splettstoesser and M.R. Wegewijs, *Nanotechnology* **21**, 272001 (2010).

⁵ J. Kondo, *Prog. Theor. Phys.* **32**, 37 (1964).

- ⁶ A. C. Hewson, *The Kondo Problem to Heavy Fermions* (Cambridge University Press, Cambridge, 1993).
- ⁷ D. Goldhaber-Gordon, H. Shtrikman, D. Mahalu, D. Abusch-Magder, U. Meirav, and M. A. Kastner, *Nature* (London) **391**, 156 (1998).
- ⁸ S. Cronenwett, T. H. Oosterkamp, and L. P. Kouwenhoven, *Science* **281**, 182 (1998).
- ⁹ M. R. Buitelaar, W. Belzig, T. Nussbaumer, B. Babic, C. Bruder, and C. Schönenberger, *Phys. Rev. Lett.* **91**, 057005 (2003).
- ¹⁰ H. I. Jorgensen, K. Grove-Rasmussen, T. Novotny, K. Flensberg, and P. E. Lindelof, *Phys. Rev. Lett.* **96**, 207003 (2006).
- ¹¹ J. A. van Dam, Y. V. Nazarov, E. P. A. M. Bakkers, S. De Franceschi, L. P. Kouwenhoven, *Nature* **442**, 667 (2006).
- ¹² T. Tsuneta, L. Lechner, and P. J. Hakonen, *Phys. Rev. Lett.* **98**, 087002 (2007).
- ¹³ M. R. Buitelaar, T. Nussbaumer, and C. Schönenberger, *Phys. Rev. Lett.* **89**, 256801 (2002).
- ¹⁴ T. Hecht, A. Weichselbaum, J. von Delft, R. Bulla, *J. Phys.: Condens. Matter* **20**, 275213 (2008).
- ¹⁵ A. N. Pasupathy, R. C. Bialczak, J. Martinek, J. E. Grose, L. A. K. Donev, P. L. McEuen, and D. C. Ralph, *Science* **306**, 86 (2004).
- ¹⁶ J. Barnaś and I. Weymann, *J. Phys.: Condens. Matter* **20**, 423202 (2008).
- ¹⁷ J. Martinek, M. Sindel, L. Borda, J. Barnaś, J. König, G. Schön, J. von Delft, *Phys. Rev. Lett.* **91**, 247202 (2003).
- ¹⁸ J. Hauptmann, J. Paaske, P. Lindelof, *Nature Phys.* **4**, 373 (2008).
- ¹⁹ M. Gaass, A. K. Hüttel, K. Kang, I. Weymann, J. von Delft, and Ch. Strunk, *Phys. Rev. Lett.* **107**, 176808 (2011).
- ²⁰ M. Sindel, L. Borda, J. Martinek, R. Bulla, J. König, G. Schön, S. Maekawa, and J. von Delft, *Phys. Rev. B* **76**, 045321 (2007).
- ²¹ I. Weymann, *Phys. Rev. B* **83**, 113306 (2011).
- ²² K. P. Wójcik, I. Weymann, and J. Barnaś, *J. Phys.: Cond. Matter* **25**, 075301 (2013).
- ²³ L. Hofstetter, A. Geresdi, M. Aagesen, J. Nygard, C. Schönenberger, S. Csonka, *Phys. Rev. Lett.* **104**, 246804 (2010).
- ²⁴ Y. Zhu, Q.-F. Sun, T.-H. Lin, *Phys. Rev. B* **65**, 024516 (2001).
- ²⁵ J.-F. Feng, S.-J. Xiong, *Phys. Rev. B* **67**, 045316 (2003).
- ²⁶ X. F. Cao, Y. Shi, X. Song, S. Zhou, H. Chen, *Phys. Rev. B* **70**, 235341 (2004).
- ²⁷ P. Zhang and Y. -X. Li, *J. Phys.: Condens. Matter* **21**, 095602 (2009).
- ²⁸ D. Futterer, M. Governale, M. G. Pala, and J. König, *Phys. Rev. B* **79**, 054505 (2009).
- ²⁹ B. Sothmann, D. Futterer, M. Governale, and J. König, *Phys. Rev. B* **82**, 094514 (2010).
- ³⁰ E. C. Siqueira, G. G. Cabrera, *Phys. Rev. B* **81**, 094526 (2010).
- ³¹ K. I. Wysokiński *J. Phys.: Condens. Matter* **24**, 335303 (2012).
- ³² K. Bocian, W. Rudziński, *Eur. Phys. J. B* **86**, 439 (2013).
- ³³ I. Weymann and P. Trocha, *Phys. Rev. B* **89**, 115305 (2014).
- ³⁴ K. G. Wilson, *Rev. Mod. Phys.* **47**, 773 (1975).
- ³⁵ R. Bulla, T. A. Costi, and T. Pruschke, *Rev. Mod. Phys.* **80**, 395 (2008).
- ³⁶ A. Weichselbaum and J. von Delft, *Phys. Rev. Lett.* **99**, 076402 (2007).
- ³⁷ We used an open-access Budapest NRG code, <http://www.phy.bme.hu/dmnrng/>; O. Legeza, C. P. Moca, A. I. Tóth, I. Weymann, G. Zaránd, [arXiv:0809.3143](https://arxiv.org/abs/0809.3143) (2008) (unpublished).
- ³⁸ P. Trocha, J. Barnaś, *Phys. Rev. B* **85**, 085408 (2012).
- ³⁹ L. D. Hicks and M. S. Dresselhaus, *Phys. Rev. B* **47**, 16631 (1993).
- ⁴⁰ T. A. Costi and V. Zlatic, *Phys. Rev. B* **81**, 235127 (2010).
- ⁴¹ T. Rejec, R. Zitko, J. Mravlje, and A. Ramsak, *Phys. Rev. B* **85**, 085117 (2012).
- ⁴² I. Weymann and J. Barnaś, *Phys. Rev. B* **88**, 085313 (2013).
- ⁴³ R. Chirla and C. P. Moca, *Phys. Rev. B* **89**, 045132 (2014).
- ⁴⁴ J. Nagamatsu, N. Nakagawa, T. Muranaka, Y. Zenitani, and J. Akimitsu, *Nature* **410**, 63 (2001).
- ⁴⁵ B. W. Heinrich, L. Braun, J. I. Pascual and K. J. Franke, *Nature Phys.* **9**, 765 (2013).
- ⁴⁶ A. V. Rozhkov and D. P. Arovas, *Phys. Rev. B* **62**, 6687 (2000).
- ⁴⁷ C. Karrasch and V. Meden, *Phys. Rev. B* **79**, 045110 (2009).
- ⁴⁸ T. Meng, S. Florens, and P. Simon, *Phys. Rev. B* **79**, 224521 (2009).
- ⁴⁹ M. Julliere, *Phys. Lett. A* **54**, 225 (1975).
- ⁵⁰ R. Zitko and T. Pruschke, *Phys. Rev. B* **79**, 085106 (2009).
- ⁵¹ V. L. Campo and L. N. Oliveira, *Phys. Rev. B* **72**, 104432 (2005).
- ⁵² J. Friedel, *Can. J. Phys.* **34**, 1190 (1956).
- ⁵³ I. Weymann, J. König, J. Martinek, J. Barnaś, and G. Schön, *Phys. Rev. B* **72**, 115334 (2005).